THE JOURNAL OF PHYSICAL CHEMISTRY C
A JOURNAL OF THE AMERICAN CHEMICAL SOCIETY

pubs.acs.org/JPCC

Article

Effects of Adsorbed OH on Pt(100)/Water Interfacial Structures and Potential

Jia-Xin Zhu, Jia-Bo Le, Marc T. M. Koper, Katharina Doblhoff-Dier,* and Jun Cheng*

Cite This: *J. Phys. Chem. C* 2021, 125, 21571−21579

Read Online

ACCESS | Metrics & More | Article Recommendations | Supporting Information

ABSTRACT: Adsorbates at the electrode change the structure of the electrode/electrolyte interface. Despite the important influence of the interfacial structure on electrochemical processes, computational investigations targeting this influence are still lacking. Even the impact of one of the most common adsorbates, namely, adsorbed OH, is so far largely unknown. In this study, we choose the Pt(100)/water interface as a model system to investigate the interfacial water structure at various OH coverages with ab initio molecular dynamics. We find that the interfacial water structure is highly sensitive to the adsorption site of OH (namely, top or bridge site) and that the preference of adsorption sites of OH is, in turn, strongly influenced by the solvation caused by interfacial water. This indicates that the structure of water is correlated with that of OH. Based on a detailed analysis, we attribute these observations to a strong hydrogen-bonding network between OH and the interfacial water. This hydrogen-bonding network also results in a complicated dependence of the interfacial potential on the OH coverage, which is governed not only by the dipole induced by OH but also by the influence the OH species have on the interfacial water structure.

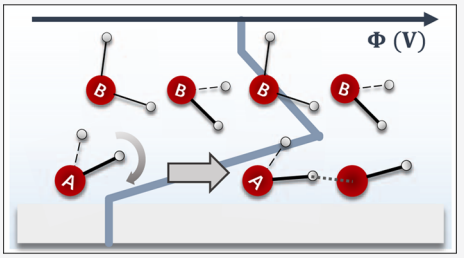

1. INTRODUCTION

In many electrochemical processes, the reaction rates and the reaction mechanisms depend on the electrolyte and the electric field applied.[1−10] One prototypical example is the strong pH-dependence of the hydrogen evolution reaction (HER),[11−18] which cannot be explained by the simplified models involving only the interaction between the reactant and the electrode under zero charge conditions. In such cases, a detailed description of the entire solid/liquid interface becomes necessary.

In electrochemistry, the adsorbates at the interface are expected to interact with their surrounding electrolyte. This interaction can be divided into two parts. On the one hand, the electrolyte, especially the solvent, can strongly influence the energetics of the adsorbates that are involved in the electrochemical reactions. One prototypical example is the adsorbed OH, which is relevant to HER, oxygen reduction reaction (ORR), and CO oxidation and has been shown to depend sensitively on (aqueous) solvation (see, e.g.,[8,19,20] for HER,[2,21−25] for ORR, and[26−29] for CO oxidation). In these and many other cases, the presence of water in the studies is essential for the reaction energetics and, in some cases,[30−33] even changes the optimal reaction pathway. On the other hand, while the solvation effect on the adsorbate is essential as mentioned above, the adsorbate, in turn, can have an impact on the surrounding solvent molecules. The description of the water itself, however, is rather simplistic in most of the previous studies and is either ice-like or includes only a few (fixed) water molecules, the positions of which are obtained from geometry optimization. Consequently, little is known on how adsorbed OH influences the structure of its surrounding water at the interface.

In this work, we aim to reveal the effect of adsorbed OH on the interfacial structure of the Pt(100)/water interface and the resulting interfacial potential. Pt(100) is a particularly interesting model system as Pt(100) does not have a double-layer window (i.e., a potential range in which the surface is bare of adsorbates) in aqueous electrolytes, and water will always dissociate spontaneously to produce adsorbed H or(and) OH.[34,35] For adsorbed H, it is known that it makes the Pt(111) surface more hydrophobic[36,37] and similar effects of H on the structure of the interfacial water are likely to occur on other metal surfaces as the hydrophobicity of the surface can be expected to make the hydrogen-bonding network less dependent on the exact type and structure of the metal. Adsorbed hydroxide OH, however, can be expected to have a less transferable and predictable influence on the interfacial structure due to the strong solvation[38] and the hydrogen-bonding network it forms with its surroundings.[39,40]

In order to model the Pt(100)/water interface in the presence of OH, ab initio molecular dynamics (AIMD) simulations are utilized. The AIMD trajectories are used to

Received: June 3, 2021
Revised: September 10, 2021
Published: September 26, 2021

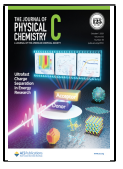

https://doi.org/10.1021/acs.jpcc.1c04895
J. Phys. Chem. C 2021, 125, 21571−21579

analyze the interfacial structure and to relate descriptors for the OH structure, such as the OH adsorption site, to the resulting changes in interfacial potential.

2. METHODS

All the density functional theory calculations are performed in CP2K/Quickstep.[41] All atoms are described by Goedecker–Teter–Hutter (GTH) pseudopotentials:[42,43] the O atom is described by the GTH-PBE-q6 pseudopotential with 2s and 2p electrons in the valence, H is described by GTH-PBE-q1, with all electrons in the valence, and Pt is described by the Pt GTH-PBE-q10 pseudopotential with 5d and 6s electrons in the valence. The DZVP-MOLOPT-SR-GTH Gaussian basis set[44] is applied to all atom types except for Pt. For Pt, we use a basis set developed for the pseudopotential Pt GTH-PBE-q10 by Le et al. for Pt(111)/water interface simulations.[45] The plane wave energy cutoff is set to 400 Ry. We use the Perdew–Burke–Ernzerhof (PBE) functional[46] to describe the exchange–correlation effect with the Grimme D3 correction[47] to account for dispersion interaction.

The Pt/water interface is described in a periodic supercell model, as shown in Figure 1. The Pt electrode is represented

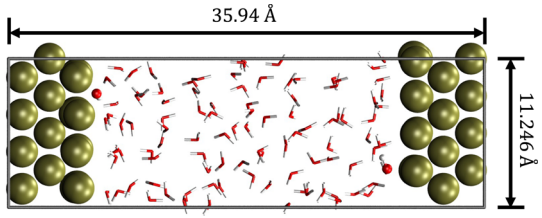

Figure 1. Side view of a snapshot of Pt(100)/water interfaces with 1/16 ML OH. OH and water molecules are represented in ball and line, respectively.

by a (4 × 4) × six-layer atomic slab, with the four nonsurface layers frozen. This slab size (11.246 × 11.246 × 35.94 Å^3) represents a good compromise between accuracy and calculation efficiency as shown via tests for the work function (see Section S1) and the water adsorption energy (see Section S2). The lattice constant is obtained from previous work (see ref 48), and the two interfaces are spaced by 26.0 Å, which are filled with water. The number of water molecules is adjusted such that the bulk water (≥9 Å from both surfaces) density in the AIMD models is close to unity, that is, (1 ± 0.05) g cm^{-3}. This results in 97 water molecules in the system.

The AIMD simulations are performed in the canonical ensemble (*NVT*) using a timestep of 0.5 fs and a target temperature of 330 K. The calculations are carried out at the Γ-point. To speed up the simulation, second-generation Car–Parrinello MD (SGCP MD)[49] is used. In the corrector step of the SGCP MD, the maximum number of iterations in the self-consistent field loop is set to 5. The Langevin friction coefficient γ_D is set equal to 0.001 fs^{-1}, while the intrinsic friction coefficient γ_L, which arises in SGCP MD, is set to 2.2 × 10^{-4} fs^{-1} for H_2O and OH and 5 × 10^{-5} fs^{-1} for Pt based on preliminary tests. At the chosen intrinsic friction coefficients, the species in the system are not observed to heat or cool. For each AIMD simulation run, an initial 5 ps or a longer time is used to pre-equilibrate the system. Then, 10 ps of AIMD is performed to obtain a converged Fermi energy and electrostatic potential (see Section S3).

In the simulations containing OH in the interface, OH is inserted at the interface after the pre-equilibration of water structures. Because bridge site OH on Pt(100) is more stable than top site OH in gas-phase calculations (Section S4), we start the calculations for OH-covered interfaces with OH adsorbed at bridge sites. The resulting structures are then re-equilibrated as described above. Since the saturation coverage of adsorbed OH on Pt(100) is around 0.29 ML,[50] we choose the range of OH coverage from 0 to 1/4 ML, corresponding to 0–4 OH species in the supercell. For Pt(100), these coverages occur at potentials at which the competitive adsorption between adsorbed O and OH can be ignored.[51]

When analyzing the trajectories, the following conventions are followed: the coverage of species (i.e., OH and water) is calculated by dividing the number of species by the number of surface atoms (16 in our cases). In the case of OH, the adsorption site of OH (namely, top and bridge site OH) is defined in the following way: first, the horizontal distance

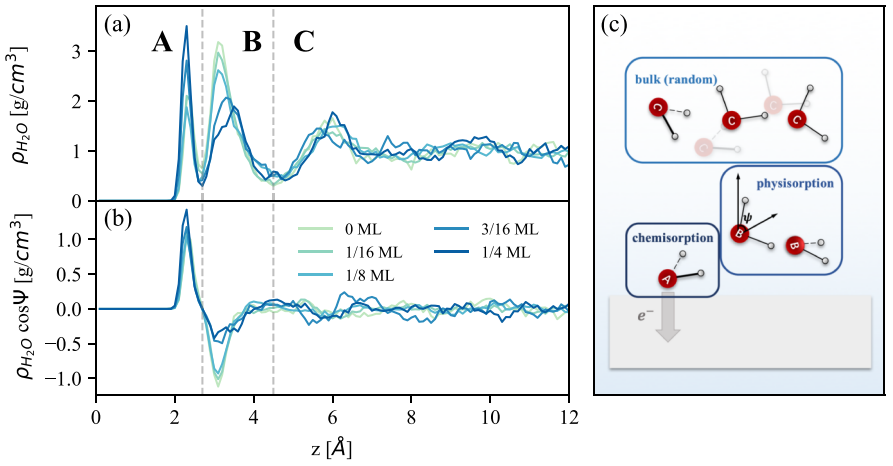

Figure 2. (a) Water density ρ_{H_2O} and (b) orientational dipole distribution ρ_{H_2O} cos ψ along the surface normal direction at different OH coverages θ_{OH}. Water can be divided into three parts (A, B, and C) according to their distances to the surfaces. (c) Schematic illustration of chemisorbed water (water A), physisorbed water (water B), and bulk water (water C) in AIMD simulations. z = 0 in (a,b) denotes the average positions of the plane through the topmost Pt layer. The position of the oxygen atom in the water molecule is used to represent the position of the water molecule in determining ρ_{H_2O} in (a,b).

https://doi.org/10.1021/acs.jpcc.1c04895
J. Phys. Chem. C 2021, 125, 21571–21579

between the oxygen atom contained in OH and the nearest top(bridge) site is calculated. Then, OH is categorized as top(bridge) site OH if it is closer to the top(bridge) site. When investigating the hydrogen-bonding network in Section 3.2.2, an O···H pair is defined as a hydrogen bond if (i) the distance between two oxygen atoms is shorter than 3.5 Å and (ii) the O···O−H angle is less than 35°.[52,53]

The AIMD trajectories provide us with direct access to the interfacial structure. Additional calculations are required to determine the interfacial potential shifts in the presence of adsorbed species. Computational details for these calculations can be found in Sections S5 and S6 in the Supporting Information.

3. RESULTS AND DISCUSSION

3.1. Interfacial Water Structure. At the electrode/electrolyte interface, the water structure can be heavily influenced by the interaction between the metal electrode and the solvent molecules. The resulting structure, which has a significant influence on the interfacial potential difference of the metal[45] and on electrocatalytic reactions,[15,54] is sensitive to the nature of both the electrode and the adsorbates at the surface. In the following, we investigate the effects of OH on the interfacial water structure on Pt(100), that is, the water density (ρ_{H_2O}) and water orientational dipole distribution ($\rho_{H_2O} \cos \psi$), as illustrated in Figure 2a,b, respectively, where ψ is the angle between the water bisector and surface normal vector. Different (experimentally relevant) OH coverages are modeled; the model of a pristine interface without any adsorbate is taken as the reference, even though it is not relevant to practical electrochemical conditions.

Overall, the water structure on Pt(100) has similar features to those observed on Pt(111).[45] Based on the water density profile as a function of distance from the surface, several water layers intersected by low-density regions can be identified. More specifically, the interfacial water can be divided into three water layers, which are labeled A (1.9−2.7 Å), B (2.7−4.5 Å), and C (≥4.5 Å) in Figure 2a. The schematic illustrations of water layers A, B, and C are shown in Figure 2c. These water layers not only differ in location but also possess different properties.

Water A transfers a fraction of electrons to the metal[45] and chemisorbs on the surfaces with an orientational dipole pointing outward from the surfaces. By contrast, the orientational dipole of the physisorbed water B points toward the surface. The rest of the water, water C, is regarded as bulk water and has a negligible net orientational dipole. On a qualitative level, the layering and the dipole orientation of the water at the surface are independent of the OH coverage (i.e., the layering is always visible and the dipole of water A always points outward from the surface, while the dipole of water B always points toward the surface). On a quantitative level, however, the OH coverage clearly influences the water density and orientational dipole distributions, and we will investigate these influences in more detail in the following.

To gain more insights into the orientational dipole of water as a function of OH coverage, the orientational distributions of water A and of water B are shown in Figure 3. At high OH coverage, water A prefers to adopt a configuration with a slightly larger angle to the surface normal of $\psi \approx 70°$ (see Figure 3a). Together with the O−H bond direction in water molecules shown in Section S7, this slightly larger angle to the surface normal can be mapped to a picture in which water A is aligned more in parallel to the surface. As for water B, its angle to the surface normal covers a wide range of values (see Figure 3b). On average, the dipole of water B points toward the surface, but there is no clear trend with increasing OH coverage.

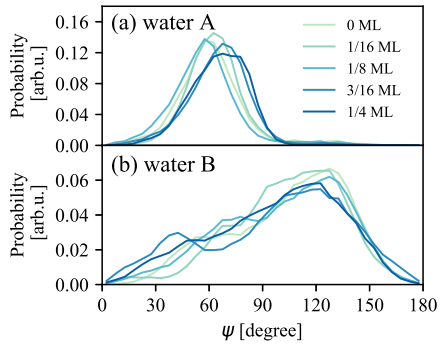

Figure 3. Normalized distribution of ψ of (a) water A and (b) water B. ψ is the angle between the water bisector and surface normal vector.

In addition to the orientational dipole, the coverage of water A and water B is also OH-coverage-dependent (see Figure 4a,b, respectively). While the coverage of water B decreases for increasing OH coverage, the coverage-dependence of water A shows a turning point: initially the coverage of water A decreases with increasing OH coverage but then increases. The decreasing coverage of water A and water B with increasing OH coverage can be rationalized as the consequence of spatial repulsion. The turning point and the sudden increase in the coverage of water A with increasing OH coverage, however, suggest the presence of a second, counteracting effect that dominates at high OH coverage. We will investigate the origin of this counteracting effect in the next section.

3.2. Origins of the OH-Coverage-Dependent Interfacial Structure. *3.2.1. OH Adsorption Site.* With increasing OH coverage, the coverage of chemisorbed water A changes and shows a turning point. In order to understand the atomic level origins of these changes in the water structure, we need to analyze the OH adsorption site and how it influences the interfacial water first.

In gas-phase calculations, OH is more stable at the bridge sites than at top sites (see Section S4). Because of this, one may expect OH to be present only in bridge sites at the interface. In the AIMD simulations, however, we observed OH in both adsorption sites (see Figure 5 and Section S8). This can be explained as the result of a stronger solvation of top site OH compared to that of bridge site OH. This manifests in the strong dependence of the OH adsorption energy (see Sections S4 and S9) and the Mulliken charge (see Section S10) on the degree of solvation.

Depending on the total OH coverage, the ratio of top and bridge site OH changes in our simulations (Figure 6). While we should be cautious not to take these ratios as accurate numbers (our calculations may not be fully converged in terms of OH adsorption sites due to the limited timescale), we may still use these numbers for a qualitative conclusion. In fact, we will try to explain the unexpected dependence of water A on the total OH coverage by analyzing it separately as a function of top and bridge site OH.

Interestingly, we find that the coverage of water A can be modeled with a high goodness fit by a simple multiple linear

https://doi.org/10.1021/acs.jpcc.1c04895
J. Phys. Chem. C 2021, 125, 21571−21579

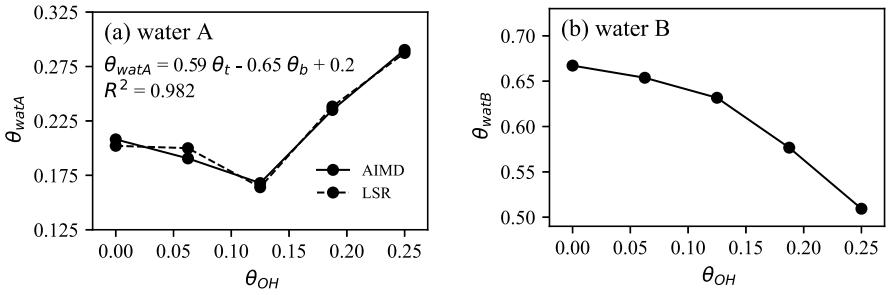

Figure 4. (a) Coverage of water A (θ_{watA}) from AIMD trajectories (solid line) and fitting data by the least square regression method (dashed line). θ_{watA}: coverage of water A, θ_t: coverage of top site OH, and θ_b: coverage of bridge site OH. (b) Coverage of water B (θ_{watB}) from AIMD trajectories.

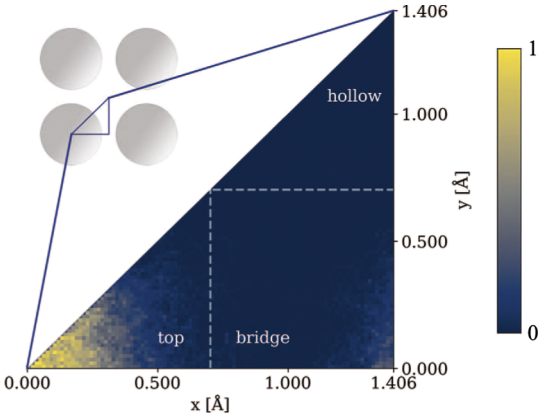

Figure 5. Heatmap for OH spatial distribution in the *xy* plane in the model with 1/4 ML OH. The lighter area indicates a higher probability of finding adsorbed OH. Coordinates of oxygen atoms in OH are used to represent the positions of OH. All the coordinates of oxygen atoms are referred to their nearest Pt atoms and folded onto an octant, as shown in the top-left corner. The color is normalized to the highest value in the heatmap, showing the relative probability of OH adsorbed at the interface.

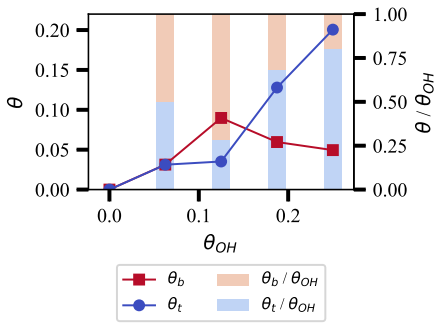

Figure 6. Left *y*-axis: bridge site OH coverage (θ_t) and top site OH coverage (θ_t). Right *y*-axis: the fraction of bridge site OH coverage (θ_t/θ_{OH}) and top site OH coverage (θ_b/θ_{OH}) proportional with all OH. The top site and bridge site OH species are defined based on the horizontal distance between the O in OH and the top/bridge site.

regression as a function of the coverage of top site and bridge site OH (see Figure 4a)

$$\theta_{watA} = \theta_{watA,0} + k_t\theta_t + k_b\theta_b \quad (1)$$

where $\theta_{watA,0}$ represents the water A coverage without OH. The other two fitting parameters k_t and k_b can be regarded as correlation factors between water A and top site or bridge site OH, respectively. We find k_t to be positive and k_b to be negative, which indicates that top site OH pulls water A toward the surface, while repulsive effects dominate for bridge site OH. Taking the observations made in this section together, we find that (i) the presence of water influences the adsorption site of OH at the interface due to solvation effects and that (ii) the adsorption site of OH has a significant effect on the coverage of water A. This suggests the presence of a site-dependent, mutual interaction between OH and the interfacial water, the origin of which we will analyze in the following.

3.2.2. Hydrogen-Bonding Network of OH at the Pt(100)/Water Interface. In the previous section, we have learnt that a complicated interplay of OH and its surrounding water exists, where the top site OH attracts water A to the surface in contrast to the bridge site OH repelling it due to spatial repulsion. So far, the mechanism of this attraction is still unclear at the atomic level. Here, we propose that a strong hydrogen-bonding network between adsorbed OH and its surrounding water accounts for this attractive interaction.

The existence of a hydrogen-bonding network between adsorbed OH and its neighboring water molecules has been reported for Pt(111).[39,51] However, Pt(111) is a special case due to the good match of its hexagonal structure to the water/OH adlayer structure. It is therefore not immediately obvious that a water/OH hydrogen-bonding network will also exist on Pt(100), which has a square lattice. However, by counting the number of hydrogen bonds formed by adsorbed OH, based on the criteria for hydrogen bonding described in Section 2, we find that adsorbed OH does indeed form hydrogen bonds with the neighboring water (see Figure 7). Furthermore, a Mulliken population analysis for the atoms in OH and water (Section S11) shows that the oxygen atoms in OH are even more negatively charged than those in water, suggesting an even stronger hydrogen-bonding network than that present between water molecules. Based on the geometry and charge, we can thus postulate that OH forms particularly strong hydrogen bonds with the surrounding water, which could account for the attraction between top site OH and water A. Based on a snapshot of the interface (see Figure S8) and previous classical MD simulation studies,[55−57] we believe these bonds to participate in the hydrogen-bonding network at the interface.

As the attraction between water A and OH varies with the adsorption sites of OH (see Section 3.2.1), we expect a difference between top and bridge site OH in the hydrogen-bonding network. Indeed, as shown in Figure 7, each top site OH can form three hydrogen bonds on average (two as acceptors and one as a donor) with its neighboring molecules, while there are only two hydrogen bonds (one acceptor and one donor) for the bridge site OH. The quantitative analysis of the hydrogen-bonding network mentioned above thus agrees with the strong attractive interaction observed between water

https://doi.org/10.1021/acs.jpcc.1c04895
J. Phys. Chem. C 2021, 125, 21571−21579

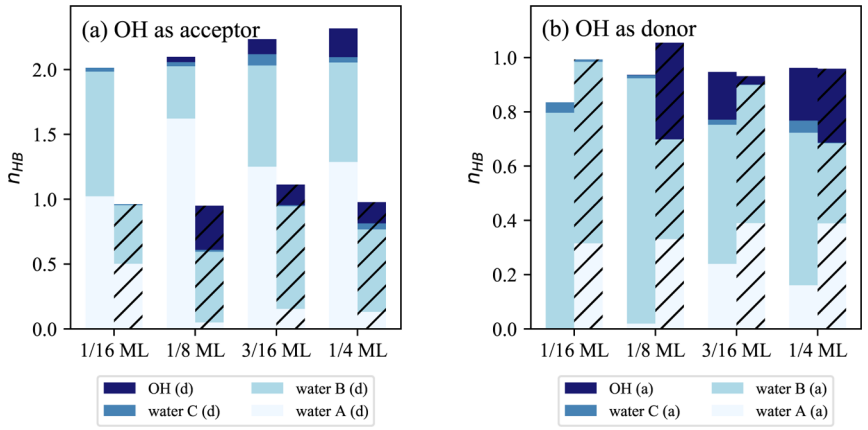

Figure 7. Comparison of hydrogen bonds (n_{HB}) of adsorbed OH as the (a) acceptor or (b) donor. Bars with and without shadow indicate bridge site and top site OH, respectively. "d" in bracket denotes the donor and "a" stands for the acceptor.

A and top site OH. Furthermore, it even explains the OH-coverage-dependent structure changes of water A (see Figure 3a) as shown in the following.

In the interfacial hydrogen-bonding network, a special HO···HOH complex with OH as an acceptor and water A as a donor is often observed for top site OH (see Figure S7). This does not only suggest a strong attraction between top site OH and water but also the observed flattening of water A at high OH coverage (see Figure 3a) as the hydrogen bond to top site OH causes the water A to be aligned more in parallel to the surface (see Section S9 in the Supporting Information). The strong hydrogen-bonding network thus explains the attractive interaction between water A and OH as well as structural changes in the interface.

3.3. Effect of OH Adsorption on Interfacial Potential.

A thorough understanding of the interfacial potential is important in electrochemistry as the interfacial potential affects adsorption energies and reaction barriers.[10,14,58] This interfacial potential can be influenced by interfacial species, and the sign and the magnitude of this species-induced shifts can be accessed via a change in the outer potential difference $\Delta\Phi$ as measured relative to the bare surface in vacuum

$$\Delta\Phi = W_e/e_0 - U_{abs} = W_e/e_0 - (U_{SHE} + U_{abs}^{SHE}) \quad (2)$$

where U_{abs} is the absolute potential of the electrode with or without adsorbates and/or water, U_{SHE} is the potential of the electrode measured versus the standard hydrogen electrode (SHE), U_{abs}^{SHE} = 4.44 V[59] is the absolute potential of the SHE, W_e = 5.49 eV is the work function of the bare metal in the computational setup used (see Section S1), and e_0 is the unit charge. Computationally, U_{abs} can be accessed if a vacuum interface is present in the simulation cell (see Section S6), while U_{SHE} can be calculated using the computational SHE (cSHE) method, as explained in Section S5.

Interfacial species can alter $\Delta\Phi$ either via their intrinsic dipole moment or by inducing electron redistribution at the interface. The interfacial potential increases if a molecule donates electrons to the electrode or if it has a dipole moment pointing outward from the surface. If, on the other hand, the surface donates electrons to the molecule or if the molecular dipole points inward, the interfacial potential will decrease. In the case of OH, two counteracting effects need to be considered: (i) OH carries a dipole moment pointing outward from the surface, contributing to a positive shift to the interfacial potential, and (ii) OH adsorption leads to partial electron transfer from the surface toward the OH species (see Section S10), contributing a negative shift to the potential. Although the relative magnitude of these two direct contributions of OH is a priori unclear, a monotonous, even linear change might be expected for the interfacial potential as a function of OH coverage in the absence of lateral interaction. Yet, the shift in interfacial potential as a function of OH coverage that we obtain in our calculations shows a strongly nonlinear behavior (see Figure 8). This indicates that either

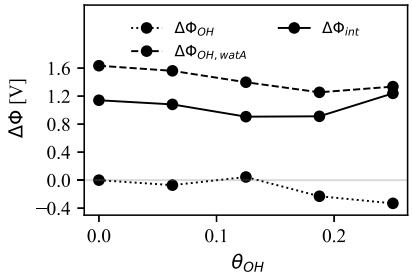

Figure 8. Interfacial potential difference $\Delta\Phi$ caused by OH ($\Delta\Phi_{OH}$, dotted line), OH and chemisorbed water A ($\Delta\Phi_{OH,watA}$, dashed line), and entire Pt/OH/water interfaces ($\Delta\Phi_{int}$, solid line) at different OH coverages. Computational details for the last one can be found in Section S5 and the others refer to Section S6 in the Supporting Information.

the behavior of OH is more intricate than that sketched above or that the interfacial water species, which we disregarded so far, have a strong, nonlinear influence on the surface potential shift. In order to disentangle these effects, we split the interfacial potential shift $\Delta\Phi$ into three parts: (i) $\Delta\Phi_{OH}$, the contribution of OH only (dotted line in Figure 8), (ii) $\Delta\Phi_{OH,watA}$, which includes the additional effect of chemisorbed water (water A) (dashed line in Figure 8), and (iii) $\Delta\Phi_{int}$, which includes the contribution of entire Pt/OH/water interfaces (solid line in Figure 8). The computational details of this separation are given in Section S6 in the Supporting Information.

$\Delta\Phi_{OH}$ (dotted line in Figure 8) describes exclusively the direct effect of the OH adsorbate on $\Delta\Phi$. Interestingly, already the OH-only-induced potential shift shows a nonlinear dependence on OH coverage, which correlates roughly with the ratio of top site to bridge site OH (compare blue bars in Figure 6 with the behavior of $\Delta\Phi_{OH}$ in Figure 8). This suggests

https://doi.org/10.1021/acs.jpcc.1c04895
J. Phys. Chem. C 2021, 125, 21571−21579

that the influence of OH on $\Delta\Phi$ varies with the OH adsorption site. Indeed, gas-phase calculations shown in Figure S12a indicate that top site OH causes a negative shift in potential, while bridge site OH induces a positive shift. This site dependence of the shift in potential can be rationalized as follows: (i) OH contributes an orientation-induced, positive shift to $\Delta\Phi$, as shown in Figure S12b. This positive shift is smaller in magnitude for top site OH than that for bridge site OH as top site OH tends to lie more in parallel to the surface than bridge site OH in AIMD simulations (see Figure S13). (ii) OH causes a charge-transfer-induced, negative shift in $\Delta\Phi$, as shown in Figure S12c. This shift is larger in magnitude for top site OH than that for bridge site OH as top site OH not only situates further from the surface but also induces a stronger charge transfer from the surface to the OH species than bridge site OH (see Figures S14 and S10). Because top site OH dominates in our calculations only at high coverage (see Figure 6), a negative shift in $\Delta\Phi_{OH}$ is only observed for high OH coverage.

The OH contribution, $\Delta\Phi_{OH}$, alone, cannot account for the overall trend observed in $\Delta\Phi_{int}$ with increasing OH coverage. Undoubtedly, the OH-coverage-dependent contribution of water is necessary to correctly capture the interfacial potential profile of the Pt/OH/water interface.

Water can influence the interfacial potential in two different ways: directly and indirectly. As for direct contributions, we consider the effect the water has on the potential due to its orientational dipole and due to the electron redistribution it causes at the interface. For water A, these effects both add a positive contribution to $\Delta\Phi$.[45] In addition to these direct effects, water A can also contribute indirectly to $\Delta\Phi$: as shown in Figure S10, water A can stabilize a larger negative charge on OH, thus enhancing the electron transfer from Pt to the OH species. This causes a negative contribution to $\Delta\Phi$. Although this effect is undoubtedly present, the direct contribution of water A is the dominant effect as the overall contribution of water A (difference between $\Delta\Phi_{OH}$ and $\Delta\Phi_{OH,watA}$ in Figure 8) is positive. These direct contributions can be expected to depend more or less linearly on the coverage of water A. Therefore, we may also expect the contribution of water A to $\Delta\Phi_{OH,watA}$ to be related to the coverage of water A. Indeed, as the coverage of water A increases at high OH coverage (see Figure 4a), the negative contribution of water A to $\Delta\Phi_{OH,wat}$ increases and even inverses the upward trend in $\Delta\Phi_{OH}$ caused by OH directly.

While $\Delta\Phi_{OH,watA}$ is sufficient to capture the qualitative trend observed in $\Delta\Phi_{int}$ as a function of OH coverage, an additional, somewhat smaller contribution is still missing (difference between the dashed and solid line in Figure 8). This smaller contribution stems mainly from the influence of the orientational dipole of water B on $\Delta\Phi$, as verified by the good linear correlation between $\Delta\Phi_{int} - \Delta\Phi_{OH,watA}$ and the orientational dipole of water B (see Figure S15).

By bringing together all the contributions mentioned above, an intricate but complete picture of the dependence of the interfacial potential on the OH coverage can be identified. Although we might have not reached full equilibrium in terms of OH adsorption sites, the interfacial potential difference as a function of OH coverage is clearly governed by a complicated interplay of the OH present at the surface and the interfacial water. Particularly, the chemisorbed water A, which is strongly influenced by the presence of OH, plays a dominant role. This finding illustrates that it is important to include this chemisorbed interfacial water layer at a reasonable (adsorbate-dependent) coverage and orientation for a qualitative analysis, while the physisorbed water layer should also be considered if an accurate and quantitative analysis of potential- or electric-field-dependent processes is sought.

4. CONCLUSIONS

In this work, we characterized the Pt(100)/water interface in the presence of adsorbed OH under zero charge conditions. Studying the interface at the atomic level, we revealed a close relationship between the properties of adsorbed OH and its surrounding water, leading to a mutual interaction of OH and the interfacial water on each other. In understanding this mutual interaction, the hydrogen-bonding network between OH and water plays an important role, allowing us to rationalize our observations. The reinforcement of the near-surface hydrogen-bonding network by adsorbed OH may influence electrochemical processes beyond a simple change in the interfacial water structure. For example, the altered hydrogen-bonding network may ease or hinder the influx of hydronium ions from the bulk solution[56,60] and may even hide active sites.[39] By providing a first analysis of the influence of OH on the interfacial water structures, our results may thus be expected to provide useful insights when studying such processes. Apart from the altered hydrogen-bonding network, the mutual interaction of OH and the interfacial water has also other far reaching effects. We find that the interfacial potential change caused by OH adsorption is dominated by OH-induced changes in the configuration of chemisorbed water rather than by OH itself. This modification of the near-surface potential drop caused by OH-induced change in the interfacial water may influence potential- and electric-field-dependent processes. An understanding of these water- and OH-induced changes of the interfacial potential may thus be relevant for accurate barrier calculations[7,14,58] and adsorption energetics.[10]

The research that we presented in this paper showcases many intriguing effects of OH and water on the Pt(100)/electrolyte interface. Nevertheless, many open questions and limitations still remain. For example, AIMD simulations, as used in this contribution, suffer from limited timescales. This issue becomes even more severe when we deal with OH adsorption at the interface due to the slow equilibration in top versus bridge site adsorption and the strong influence this has on the interfacial water structure. Fortunately, the emergence of machine learning approaches[61,62] and their combination with concurrent learning[63] can be used to extend the timescale of MD simulations to a few nanoseconds, providing us with a new way to overcome these difficulties. Another issue arises when trying to capture the pH effect in our system. Due to the high cost of free energy calculations, including pH effects in AIMD simulations is still challenging. Establishing a model for the electric double layer that can correctly capture the potential versus distance relationship at constant pH will thus remain a problem. In awaiting simulation tools that will allow us to directly access these properties, the analysis presented in this paper will hopefully prove to be a useful tool allowing limited insights into the happenings at an OH-covered Pt surface.

■ ASSOCIATED CONTENT

Supporting Information

The Supporting Information is available free of charge at https://pubs.acs.org/doi/10.1021/acs.jpcc.1c04895.

https://doi.org/10.1021/acs.jpcc.1c04895
J. Phys. Chem. C 2021, 125, 21571−21579

Work function of Pt(100); water adsorption energy on Pt(100); Fermi level and electrostatic potential convergence in AIMD simulations; adsorption energy of top site and bridge site OH on the metal surface in vacuum; brief description of the cSHE method; species-resolved interfacial potential shift; configurations of chemisorbed water; OH spatial distribution in *xy* planes; OH adsorption site and geometry based on microsolvation models; Mulliken charge analyses on top site and bridge site OH with different degrees of solvation of OH; Mulliken charge on O and H atoms in OH and water A; gas-phase calculations for OH-covered surfaces; OH spatial distributions in the *z* direction; correlation between the physisorbed water dipole and its resulting potential shift; and basis set used for Pt (PDF)

AUTHOR INFORMATION

Corresponding Authors

Katharina Doblhoff-Dier − *Leiden Institute of Chemistry, Leiden University, Leiden 2300RA, The Netherlands;* orcid.org/0000-0002-5981-9438; Email: k.doblhoff-dier@lic.leidenuniv.nl

Jun Cheng − *State Key Laboratory of Physical Chemistry of Solid Surfaces, iChEM, College of Chemistry and Chemical Engineering, Xiamen University, Xiamen 361005, China;* orcid.org/0000-0001-6971-0797; Email: chengjun@xmu.edu.cn

Authors

Jia-Xin Zhu − *State Key Laboratory of Physical Chemistry of Solid Surfaces, iChEM, College of Chemistry and Chemical Engineering, Xiamen University, Xiamen 361005, China;* orcid.org/0000-0002-3471-4728

Jia-Bo Le − *Ningbo Institute of Materials Technology and Engineering, Chinese Academy of Sciences, Ningbo 315201, China*

Marc T. M. Koper − *Leiden Institute of Chemistry, Leiden University, Leiden 2300RA, The Netherlands;* orcid.org/0000-0001-6777-4594

Complete contact information is available at: https://pubs.acs.org/10.1021/acs.jpcc.1c04895

Notes

The authors declare no competing financial interest.

ACKNOWLEDGMENTS

J.-X.Z. acknowledges funding from the top-notch students scientific development pilot program of Ministry of Education, China. J.C. is grateful for the funding support from the National Natural Science Foundation of China (grant nos. 21861132015, 21991151, 21991150, and 22021001).

REFERENCES

(1) Wasileski, S. A.; Koper, M. T. M.; Weaver, M. J. Field-dependent electrode-chemisorbate bonding: Sensitivity of vibrational stark effect and binding energetics to nature of surface coordination. *J. Am. Chem. Soc.* **2002**, *124*, 2796−2805.

(2) Hyman, M. P.; Medlin, J. W. Theoretical study of the adsorption and dissociation of oxygen on Pt(111) in the presence of homogeneous electric fields. *J. Phys. Chem. B* **2005**, *109*, 6304−6310.

(3) Karlberg, G. S.; Jaramillo, T. F.; Skúlason, E.; Rossmeisl, J.; Bligaard, T.; Nørskov, J. K. Cyclic voltammograms for H on Pt(111) and Pt(100) from first principles. *Phys. Rev. Lett.* **2007**, *99*, 126101.

(4) Mamatkulov, M.; Filhol, J.-S. An ab initio study of electrochemical vs. electromechanical properties: The case of CO adsorbed on a Pt(111) surface. *Phys. Chem. Chem. Phys.* **2011**, *13*, 7675−7684.

(5) Montoya, J. H.; Shi, C.; Chan, K.; Nørskov, J. K. Theoretical insights into a CO dimerization mechanism in CO2 electroreduction. *J. Phys. Chem. Lett.* **2015**, *6*, 2032−2037.

(6) McCrum, I. T.; Janik, M. J. pH and Alkali Cation Effects on the Pt Cyclic Voltammogram Explained Using Density Functional Theory. *J. Phys. Chem. C* **2016**, *120*, 457−471.

(7) Chen, L. D.; Urushihara, M.; Chan, K.; Nørskov, J. K. Electric Field Effects in Electrochemical CO2 Reduction. *ACS Catal.* **2016**, *6*, 7133−7139.

(8) McCrum, I. T.; Chen, X.; Schwarz, K. A.; Janik, M. J.; Koper, M. T. M. Effect of Step Density and Orientation on the Apparent pH Dependence of Hydrogen and Hydroxide Adsorption on Stepped Platinum Surfaces. *J. Phys. Chem. C* **2018**, *122*, 16756−16764.

(9) Sarabia, F. J.; Sebastián-Pascual, P.; Koper, M. T. M.; Climent, V.; Feliu, J. M. Effect of the Interfacial Water Structure on the Hydrogen Evolution Reaction on Pt(111) Modified with Different Nickel Hydroxide Coverages in Alkaline Media. *ACS Appl. Mater. Interfaces* **2019**, *11*, 613−623.

(10) Gauthier, J. A.; Dickens, C. F.; Heenen, H. H.; Vijay, S.; Ringe, S.; Chan, K. Unified Approach to Implicit and Explicit Solvent Simulations of Electrochemical Reaction Energetics. *J. Chem. Theory Comput.* **2019**, *15*, 6895−6906.

(11) Durst, J.; Siebel, A.; Simon, C.; Hasché, F.; Herranz, J.; Gasteiger, H. A. New insights into the electrochemical hydrogen oxidation and evolution reaction mechanism. *Energy Environ. Sci.* **2014**, *7*, 2255−2260.

(12) Sheng, W.; Zhuang, Z.; Gao, M.; Zheng, J.; Chen, J. G.; Yan, Y. Correlating hydrogen oxidation and evolution activity on platinum at different pH with measured hydrogen binding energy. *Nat. Commun.* **2015**, *6*, 5848.

(13) Rossmeisl, J.; Chan, K.; Skúlason, E.; Björketun, M. E.; Tripkovic, V. On the pH dependence of electrochemical proton transfer barriers. *Catal. Today* **2016**, *262*, 36−40.

(14) Chan, K.; Nørskov, J. K. Potential Dependence of Electrochemical Barriers from ab Initio Calculations. *J. Phys. Chem. Lett.* **2016**, *7*, 1686−1690.

(15) Ledezma-Yanez, I.; Wallace, W. D. Z.; Sebastián-Pascual, P.; Climent, V.; Feliu, J. M.; Koper, M. T. M. Interfacial water reorganization as a pH-dependent descriptor of the hydrogen evolution rate on platinum electrodes. *Nat. Energy* **2017**, *2*, 17031.

(16) Cheng, T.; Wang, L.; Merinov, B. V.; Goddard, W. A. Explanation of Dramatic pH-Dependence of Hydrogen Binding on Noble Metal Electrode: Greatly Weakened Water Adsorption at High pH. *J. Am. Chem. Soc.* **2018**, *140*, 7787−7790.

(17) Liu, E.; Li, J.; Jiao, L.; Doan, H. T. T.; Liu, Z.; Zhao, Z.; Huang, Y.; Abraham, K. M.; Mukerjee, S.; Jia, Q. Unifying the Hydrogen Evolution and Oxidation Reactions Kinetics in Base by Identifying the Catalytic Roles of Hydroxyl-Water-Cation Adducts. *J. Am. Chem. Soc.* **2019**, *141*, 3232−3239.

(18) Lamoureux, P. S.; Singh, A. R.; Chan, K. PH Effects on Hydrogen Evolution and Oxidation over Pt(111): Insights from First-Principles. *ACS Catal.* **2019**, *9*, 6194−6201.

(19) Chen, X.; McCrum, I. T.; Schwarz, K. A.; Janik, M. J.; Koper, M. T. M. Co-adsorption of Cations as the Cause of the Apparent pH Dependence of Hydrogen Adsorption on a Stepped Platinum Single-Crystal Electrode. *Angew. Chem., Int. Ed.* **2017**, *56*, 15025−15029.

(20) McCrum, I. T.; Koper, M. T. M. The role of adsorbed hydroxide in hydrogen evolution reaction kinetics on modified platinum. *Nat. Energy* **2020**, *5*, 891−899.

(21) Nørskov, J. K.; Rossmeisl, J.; Logadottir, A.; Lindqvist, L.; Kitchin, J. R.; Bligaard, T.; Jónsson, H. Origin of the overpotential for oxygen reduction at a fuel-cell cathode. *J. Phys. Chem. B* **2004**, *108*, 17886−17892.

(22) Karlberg, G. S.; Rossmeisl, J.; Nørskov, J. K. Estimations of electric field effects on the oxygen reduction reaction based on the

density functional theory. *Phys. Chem. Chem. Phys.* **2007**, *9*, 5158−5161.
(23) Strmcnik, D.; Kodama, K.; Van Der Vliet, D.; Greeley, J.; Stamenkovic, V. R.; Marković, N. M. The role of non-covalent interactions in electrocatalytic fuel-cell reactions on platinum. *Nat. Chem.* **2009**, *1*, 466−472.
(24) Strmcnik, D.; Van Der Vliet, D. F.; Chang, K.-C.; Komanicky, V.; Kodama, K.; You, H.; Stamenkovic, V. R.; Marković, N. M. Effects of Li^+, K^+, and Ba^{2+} cations on the ORR at model and high surface area Pt and Au surfaces in alkaline solutions. *J. Phys. Chem. Lett.* **2011**, *2*, 2733−2736.
(25) Dong, J.-C.; Zhang, X.-G.; Briega-Martos, V.; Jin, X.; Yang, J.; Chen, S.; Yang, Z.-L.; Wu, D.-Y.; Feliu, J. M.; Williams, C. T.; et al. In situ Raman spectroscopic evidence for oxygen reduction reaction intermediates at platinum single-crystal surfaces. *Nat. Energy* **2019**, *4*, 60−67.
(26) Gilman, S. The mechanism of electrochemical oxidation of carbon monoxide and methanol on platinum. II. The "Reactant-Pair" mechanism for electrochemical oxidation of carbon monoxide and methanol. *J. Phys. Chem.* **1964**, *68*, 70−80.
(27) Gong, X.-Q.; Hu, P.; Raval, R. The catalytic role of water in CO oxidation. *J. Chem. Phys.* **2003**, *119*, 6324−6334.
(28) Desai, S.; Neurock, M. A first principles analysis of CO oxidation over Pt and Pt 66.7%Ru33.3% (111) surfaces. *Electrochim. Acta* **2003**, *48*, 3759−3773.
(29) Tiwari, A.; Heenen, H. H.; Bjørnlund, A. S.; Hochfilzer, D.; Chan, K.; Horch, S. Electrochemical Oxidation of CO on Cu Single Crystals under Alkaline Conditions. *ACS Energy Lett.* **2020**, *5*, 3437−3442.
(30) Desai, S. K.; Neurock, M. First-principles study of the role of solvent in the dissociation of water over a Pt-Ru alloy. *Phys. Rev. B: Condens. Matter Mater. Phys.* **2003**, *68*, 075420.
(31) Sheng, T.; Lin, W.-F.; Hardacre, C.; Hu, P. Role of water and adsorbed hydroxyls on ethanol electrochemistry on Pd: New mechanism, active centers, and energetics for direct ethanol fuel cell running in alkaline medium. *J. Phys. Chem. C* **2014**, *118*, 5762−5772.
(32) Sakong, S.; Groß, A. Methanol Oxidation on Pt(111) from First-Principles in Heterogeneous and Electrocatalysis. *Electrocatalysis* **2017**, *8*, 577−586.
(33) Schweitzer, B.; Steinmann, S. N.; Michel, C. Can micro-solvation effects be estimated from vacuum computations? A case-study of alcohol decomposition at the H2O/Pt(111) interface. *Phys. Chem. Chem. Phys.* **2019**, *21*, 5368−5377.
(34) Rodes, A.; Zamakhchari, M. A.; El Achi, K.; Clavilier, J. Electrochemical behaviour of Pt(100) in various acidic media. *J. Electroanal. Chem.* **1991**, *305*, 115−129.
(35) Janik, M. J.; McCrum, I. T.; Koper, M. T. M. On the presence of surface bound hydroxyl species on polycrystalline Pt electrodes in the "hydrogen potential region" (0−0.4 V-RHE). *J. Catal.* **2018**, *367*, 332−337.
(36) Sakong, S.; Groß, A. The electric double layer at metal-water interfaces revisited based on a charge polarization scheme. *J. Chem. Phys.* **2018**, *149*, 084705.
(37) Roman, T.; Groß, A. Structure of water layers on hydrogen-covered Pt electrodes. *Catal. Today* **2013**, *202*, 183−190.
(38) Koper, M. T. M. Blank voltammetry of hexagonal surfaces of Pt-group metal electrodes: Comparison to density functional theory calculations and ultra-high vacuum experiments on water dissociation. *Electrochim. Acta* **2011**, *56*, 10645−10651.
(39) Kristoffersen, H. H.; Vegge, T.; Hansen, H. A. OH formation and H_2 adsorption at the liquid water-Pt(111) interface. *Chem. Sci.* **2018**, *9*, 6912−6921.
(40) Heenen, H. H.; Gauthier, J. A.; Kristoffersen, H. H.; Ludwig, T.; Chan, K. Solvation at metal/water interfaces: An ab initio molecular dynamics benchmark of common computational approaches. *J. Chem. Phys.* **2020**, *152*, 144703.
(41) Vandevondele, J.; Krack, M.; Mohamed, F.; Parrinello, M.; Chassaing, T.; Hutter, J. Quickstep: Fast and accurate density functional calculations using a mixed Gaussian and plane waves approach. *Comput. Phys. Commun.* **2005**, *167*, 103−128.
(42) Goedecker, S.; Teter, M.; Hutter, J. Separable dual-space Gaussian pseudopotentials. *Phys. Rev. B: Condens. Matter Mater. Phys.* **1996**, *54*, 1703−1710.
(43) Hartwigsen, C.; Goedecker, S.; Hutter, J. Relativistic separable dual-space Gaussian pseudopotentials from H to Rn. *Phys. Rev. B: Condens. Matter Mater. Phys.* **1998**, *58*, 3641−3662.
(44) VandeVondele, J.; Hutter, J. Gaussian basis sets for accurate calculations on molecular systems in gas and condensed phases. *J. Chem. Phys.* **2007**, *127*, 114105.
(45) Le, J.; Iannuzzi, M.; Cuesta, A.; Cheng, J. Determining Potentials of Zero Charge of Metal Electrodes versus the Standard Hydrogen Electrode from Density-Functional-Theory-Based Molecular Dynamics. *Phys. Rev. Lett.* **2017**, *119*, 016801.
(46) Perdew, J. P.; Burke, K.; Ernzerhof, M. Generalized gradient approximation made simple. *Phys. Rev. Lett.* **1996**, *77*, 3865−3868.
(47) Grimme, S.; Antony, J.; Ehrlich, S.; Krieg, H. A consistent and accurate ab initio parametrization of density functional dispersion correction (DFT-D) for the 94 elements H-Pu. *J. Chem. Phys.* **2010**, *132*, 154104.
(48) Le, J.; Cuesta, A.; Cheng, J. The structure of metal-water interface at the potential of zero charge from density functional theory-based molecular dynamics. *J. Electroanal. Chem.* **2018**, *819*, 87−94.
(49) Kühne, T. D.; Krack, M.; Mohamed, F. R.; Parrinello, M. Efficient and accurate car-parrinello-like approach to born-oppenheimer molecular dynamics. *Phys. Rev. Lett.* **2007**, *98*, 066401−4.
(50) Garcia-Araez, N.; Climent, V.; Feliu, J. M. Analysis of temperature effects on hydrogen and OH adsorption on Pt(1 1 1), Pt(1 0 0) and Pt(1 1 0) by means of Gibbs thermodynamics. *J. Electroanal. Chem.* **2010**, *649*, 69−82.
(51) Climent, V.; Gómez, R.; Orts, J. M.; Feliu, J. M. Thermodynamic analysis of the temperature dependence of OH adsorption on Pt(111) and Pt(100) electrodes in acidic media in the absence of specific anion adsorption. *J. Phys. Chem. B* **2006**, *110*, 11344−11351.
(52) Cicero, G.; Grossman, J. C.; Schwegler, E.; Gygi, F.; Galli, G. Water confined in nanotubes and between graphene sheets: A first principle study. *J. Am. Chem. Soc.* **2008**, *130*, 1871−1878.
(53) Velasco-Velez, J.-J.; Wu, C. H.; Pascal, T. A.; Wan, L. F.; Guo, J.; Prendergast, D.; Salmeron, M. The structure of interfacial water on gold electrodes studied by x-ray absorption spectroscopy. *Science* **2014**, *346*, 831−834.
(54) Casalongue, H. S.; Kaya, S.; Viswanathan, V.; Miller, D. J.; Friebel, D.; Hansen, H. A.; Nørskov, J. K.; Nilsson, A.; Ogasawara, H. Direct observation of the oxygenated species during oxygen reduction on a platinum fuel cell cathode. *Nat. Commun.* **2013**, *4*, 2817.
(55) Willard, A. P.; Limmer, D. T.; Madden, P. A.; Chandler, D. Characterizing heterogeneous dynamics at hydrated electrode surfaces. *J. Chem. Phys.* **2013**, *138*, 184702.
(56) Limmer, D. T.; Willard, A. P.; Madden, P.; Chandler, D. Hydration of metal surfaces can be dynamically heterogeneous and hydrophobic. *Proc. Natl. Acad. Sci. U.S.A.* **2013**, *110*, 4200−4205.
(57) Limmer, D. T.; Willard, A. P.; Madden, P. A.; Chandler, D. Water exchange at a hydrated platinum electrode is rare and collective. *J. Phys. Chem. C* **2015**, *119*, 24016−24024.
(58) Lindgren, P.; Kastlunger, G.; Peterson, A. A. A Challenge to the G ∼ 0 Interpretation of Hydrogen Evolution. *ACS Catal.* **2020**, *10*, 121−128.
(59) Trasatti, S. The absolute electrode potential: an explanatory note (Recommendations 1986). *Pure Appl. Chem.* **1986**, *58*, 955−966.
(60) Serva, A.; Salanne, M.; Havenith, M.; Pezzotti, S. Size dependence of hydrophobic hydration at electrified gold/water interfaces. *Proc. Natl. Acad. Sci. U.S.A.* **2021**, *118*, No. e2023867118.
(61) Wang, H.; Zhang, L.; Han, J.; E, W. DeePMD-kit: A deep learning package for many-body potential energy representation and molecular dynamics. *Comput. Phys. Commun.* **2018**, *228*, 178−184.

https://doi.org/10.1021/acs.jpcc.1c04895
J. Phys. Chem. C 2021, 125, 21571−21579

(62) Grisafi, A.; Ceriotti, M. Incorporating long-range physics in atomic-scale machine learning. *J. Chem. Phys.* **2019**, *151*, 204105.
(63) Zhang, L.; Lin, D.-Y.; Wang, H.; Car, R.; E, W. Active learning of uniformly accurate interatomic potentials for materials simulation. *Phys. Rev. Mater.* **2019**, *3*, 23804.

https://doi.org/10.1021/acs.jpcc.1c04895
J. Phys. Chem. C 2021, 125, 21571−21579